Flower-like AuPtPd-Fe₃O₄ Nanocatalyst for Electrochemical Removal of Humic Acids and Cr(VI)

Maria Sarno, Carmela Scudieri[*], Eleonora Ponticorvo

Department of Industrial Engineering and Centre NANO_MATES University of Salerno, Via Giovanni Paolo II ,132 - 84084 Fisciano (SA), Italy
cscudieri@unisa.it

Flower-like AuPtPd-Fe₃O₄ new nanohybrid prepared through a scalable synthetic approach was tested for the effective and simultaneous removal of Humic Acids and Cr (VI). Field emission scanning electron microscopy (FESEM) equipped with an energy dispersive X-ray (EDX) probe, X-ray diffractometer (XRD) and thermogravimetric analysis (TG-DTG) were used for characterization. The nanocatalyst, at the end of the preparation process, results dispersible in water. Calibration equations were plotted for the removal evaluation of Cr(VI) and Humic Acids in water samples. Electrochemical tests were carried out at pH 3.0 and 30 mA. Humic Acids were highly mineralized with TOC removal efficiency of 95%. In 3 h, 99 % of total Cr was removed.

1. Introduction

Humic acids (HAs) is one of the principal components of natural humic substances (HS) that are originated from the decomposition of various plant materials and animal residues, so it is considered to be the dominant constituent of dissolved organic matter (DOM) not only in drinking water source but also in other natural water resources (Costa et al., 2011). HAs are composed of aliphatic or aromatic organic macromolecules with carboxylic acid group, phenolic hydroxyl group, and quinone groups (Chen et al., 2003). The presence of HAs in potable water also result in negative effect on water quality by causing color, taste and odor problems (Lin et al., 2012). Moreover, these compounds are widely recognized as precursors of potentially carcinogenic disinfection by-products (DBPs), e.g. trihalomethanes formation during chlorine disinfection process (Trellu et al., 2016). Therefore, humic acid poisoning of drinking water sources is an urgent problem requiring easy and efficient removal strategies. Hexavalent chromium (Cr(VI)), is mobile in the environment and is highly toxic. Cr(VI) can easily penetrate the cell wall and exerts its noxious influence in the cell itself, being also a source of various cancer diseases (Gil et al., 2006). As a human carcinogen, Cr(VI) compounds can cause cancer at tissue sites, bone cancer, and leukemia due to high exposure from chrome tanning, chrome plating, Cr(VI) pigments, and arc welding. Due to the presence of chromium in aqueous systems, many scholars have studied this material and its toxic properties. Cr (VI) has been classified as Group A inhalation carcinogen by US EPA and Group I human carcinogen by the IARC (International Agency for Research on Cancer) (Wang et al., 2016), resulting into strictly regulated Cr (VI) level, which must be in drinking water lower than 0.05 mg/L (Gil et al., 2006). In addition, anion Cr (VI) is readily to enter and migrate in the soil and aquatic environments, leading to a tremendous threat to water supply sources (e.g. surface water and groundwater). On another side, the increasing uses of chromium in industries have led to a large amount of effluents that contain Cr (VI), which thus makes possible the coexistence of HAs and Cr (VI) in natural water bodies. The widespread presence of humic acids (HAs) and chromium (Cr) in aquatic systems and drinking water sources is a serious threat to the environment and human being. However, very few studies on the potential interaction and simultaneous removal of these two types of contaminants have been conducted. Different catalysts have been proposed and studied for the removal of HAs and Cr (VI) (Celebi et al., 2016). On the hand, nanotechnology offers also in this field a real opportunity of innovation, supplying new structure and morphology able to increase catalytic activity and selectivity for the simultaneous removal of both humic acids and chromium.

Here, in order to exploit the role on the selectivity of Pt and Au, for the first time, we propose a flower-like AuPtPd-Fe$_3$O$_4$ nanoparticles for the effective and simultaneous removal of HAs and Cr (VI). The catalyst selectivity is dominated by Pt and Au species, in which Au fatherly improve the catalyst tendency to form H$_2$O$_2$ instead of H$_2$ combustion (Sterchele et al., 2013; Sarno et al., 2018a). HAs were efficiently mineralized, as revealed by a total organic carbon removal efficiency and Cr(VI) was completely reduced.

2. Experimental

HAs were purchased from Sigma Aldrich. Potassium dichromate, Platinum(II) acetylacetonate, Palladium(II) acetylacetonate, Gold(III) chloride hydrate, oleic acid, 1,2-hexadecanediol, 1-octadecene and citric acid were analytic grade from Sigma Aldrich Co., used as received. AuPtPd-Fe$_3$O$_4$ nanocomposite was obtained by a one-step method. In particular, before the synthesis, Platinum(II) acetylacetonate (0.1 mmol), Palladium(II) acetylacetonate (0.1 mmol), Gold(III) chloride hydrate (0.1 mmol), Iron(III) acetylacetonate (2 mmol), oleic acid (12 mmol), 1,2-hexadecanediol (10 mmol) and 20 ml of 1-octadecene were intimately mixed by sonication. After, the mixture was heated to 200 °C for 2 h under N$_2$ flow, and furthermore heated to reflux (~285 °C) for 1 h. The formed black-brown mixture was cooled to room temperature by removing the heat source. To favour the dispersion of the NPs in the electrochemical medium a ligand exchange with citric acid (CA) was promoted (Sarno et al., 2017a; Sarno et al., 2018b). The characterization was obtained by the combined use of different techniques. Field emission scanning electron microscopy (FESEM) images were obtained by the use of a Phenom electron microscope, equipped with an energy dispersive X-ray (EDX) probe. A Bruker D8 X-ray diffractometer with a monochromatic CuKα radiation was used for measurements of powder diffraction profiles. Thermogravimetric analysis (TG-DTG) at a 10 K/min heating rate in flowing air was performed with a SDTQ 600 Analyzer (TA Instruments) (Trezza et al., 2008). Due to the complexity of the HAs organic matter, the evolution of the reaction was determined by a global parameter, i.e. the total organic carbon (TOC) content of the solution (TOC sol), in mg/L. Samples were collected at different time points during the electrolysis. TOC was measured by using a Shimadzu TOC-V analyzer. To prepare the HAs solution, a purification step of commercial HAs was performed, similarly to the protocol of Arai et al. (Arai et al., 1986). The stock solution was prepared by dissolving commercial HAs in distilled water at pH 3. This solution was filtered through Whatman GF/F filter (0.7 µm as pore diameter). Then, HAs were precipitated by decreasing pH to 1.2 and the solution was centrifuged at 3000 rpm during 20 min. All electrochemical tests were carried out during 6 h in a 100 ml batch electrochemical cell using Autolab PGSTAT302N potentiostat. The anode material was boron-doped diamond (BDD) thin-film onto a Nb substrate and the cathode material was a Pt foil. Electrodes were set up with a gap of 2 cm between the anode and the cathode. For a typical electrochemical test, considering that in a natural water system, HAs are present in concentrations ranging from 0.1 to 200 mg/L (Kinniburgh et al., 1996), while, the concentration of Cr(VI) depends on the adsorption characteristics of the soil surfaces, a solution containing an initial TOC concentration of 120 mg/L and 50 mg/L of Cr(VI) (e.g. tannery wastewater) was prepared. The pH solution was adjusted using dilute H$_2$SO$_4$ or 1.0 M NaOH before electrolysis. After adding 0.8 g of AuPtPd-Fe$_3$O$_4$. The solution was stirred at 300 rpm using a magnetic stirring bar coated with Teflon throughout the experiment. The aqueous samples were withdrawn for analysis at determined time intervals.

3. Results and discussion

Figure 1 shows XRD pattern of the obtained products. The diffraction peaks at 35.46° (311), 43.01° (400), 52.91° (422), 57.02° (511) and 62.64° (440) are in agreement with the JCPDS file of magnetite (JCPDS No. 75-0033) (Sun et al., 2009; Xu et al., 2009; Ban et al., 2010; Ghandoor et al., 2012). The peaks (Wang et al., 2011) at 38.42°, 44.49°, 64.88°, 78.02°, 82.93° can be indexed to the Au (111), (200), (220), (311) and (222) respectively crystal faces (JCPDS No. 04-0784) (Ren et al., 2015). The blue arrows in the graph of Figure 1 indicate the 2θ° positions of a Pt and Pd alloy. Indeed, the peaks are at higher and lower angles if compared with pure Pt and pure Pd, respectively (Sarno et al., 2017b, Sarno et al., 2018c).

The Fe$_3$O$_4$ crystalline size, measured by Scherrer's equation (Ciambelli et al., 2004) applied at (440) peak of Fe$_3$O$_4$, was found to be ~ 16.9 nm. The lattice parameter "a" and interplanar d spacing d$_{hkl}$ (Sarno et al., 2017b) were found quite close to the standard lattice parameter of magnetite and relatively far from the one of maghemite, which indicates that the as-synthesized iron oxide particles are in magnetite phase (Xu et al., 2009). The Scherrer's equation applied at the other Fe$_3$O$_4$ diffraction peaks confirms the quasi-spherical nature of the component in the nanocomposite. The SEM images (see Figure 2a,b) for AuPtPd-Fe$_3$O$_4$ illustrate the nanocomposite, which is constituted of nanoparticles ~ 40 nm in diameter. Each nanoparticle has a flower-like morphology, with a magnetite core and numerous as also confirmed by TEM images not shown

here. The nanocomposites, prepared in a one-step procedure, consists of nanoparticles with grain size of about 40 nm, constituted of a magnetite core ~20 nm and petals of PtPd and Au, see the insert in Figure 2b.
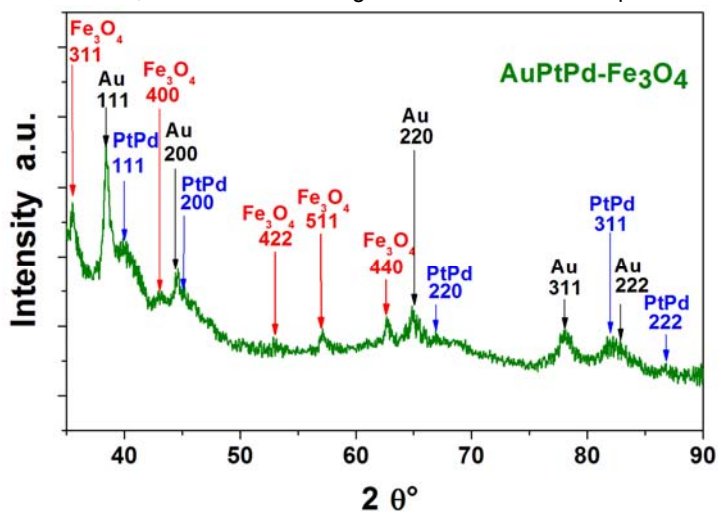

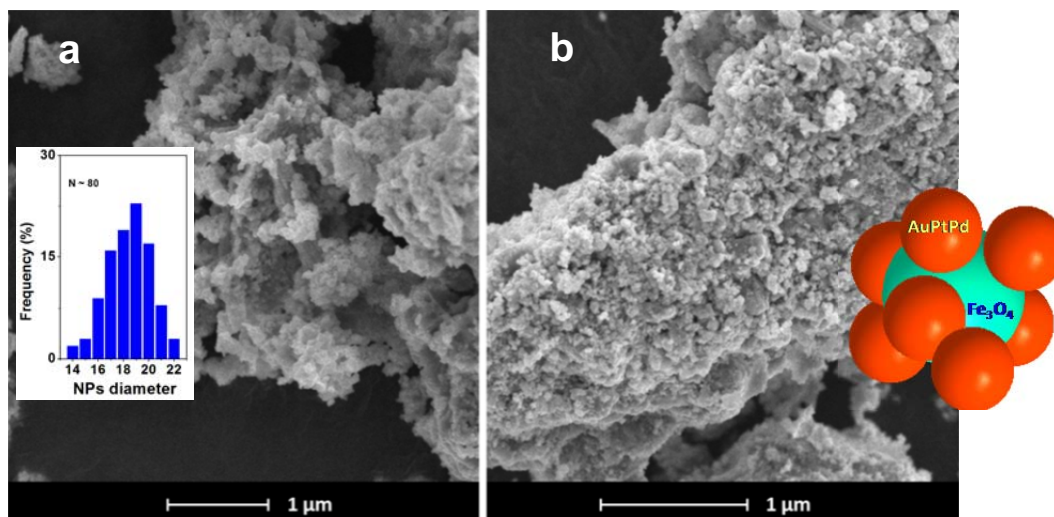*Figure 1 XRD spectrum of AuPtPd-Fe$_3$O$_4$ nanocomposite*

Figure 2 SEM (a,b) images of AuPtPd-Fe$_3$O$_4$ nanocomposite; Fe$_3$O$_4$ size distribution histogram and schematic representation of AuPtPd-Fe$_3$O$_4$ nanocomposite in the inserts.

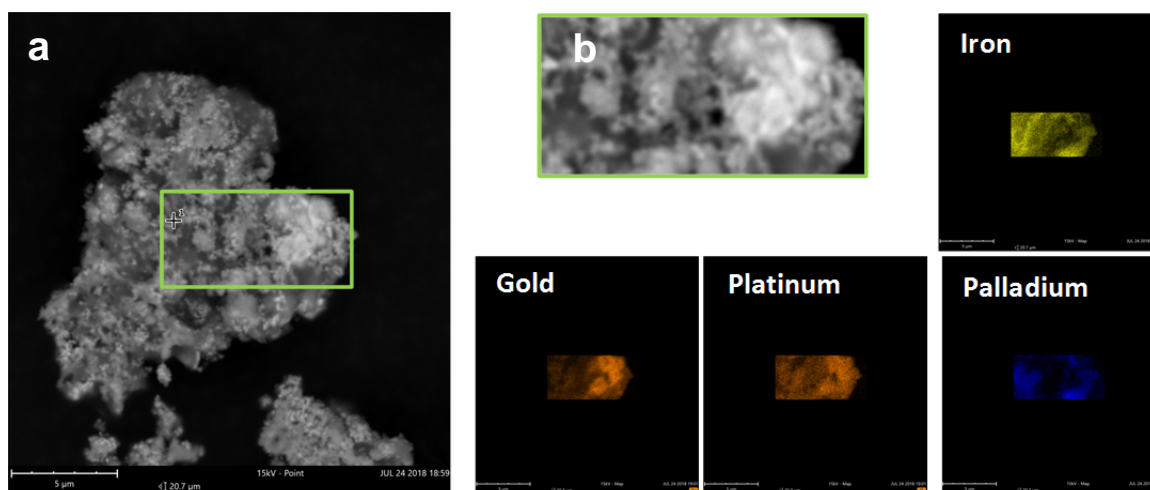*Figure 3 Characterization of AuPtPd-Fe$_3$O$_4$ nanocomposite using SEM-EDX.*

In addition, to further investigate the Pt, Pd, Au and Fe_3O_4 arrangement, in Figure 3 the SEM images at increasing magnification and the corresponding EDX maps for each metal reveal that platinum, palladium, gold and magnetite are homogeneously distributed in the sample. Figure 4a shows the TG-DTG results obtained on the as prepared $AuPtPd-Fe_3O_4$ nanocomposite, after an initial weight loss, due to adsorbed water, a weight loss due to surfactant can be observed, then the sample stays stable up to 1000 °C (Sarno et al., 2017b; Ferrara et al., 2007). The UV–vis absorbance spectra of chromium and humic acids alone, and a chromium-humic acids mixture in aqueous solutions were shown in Figure 4b.
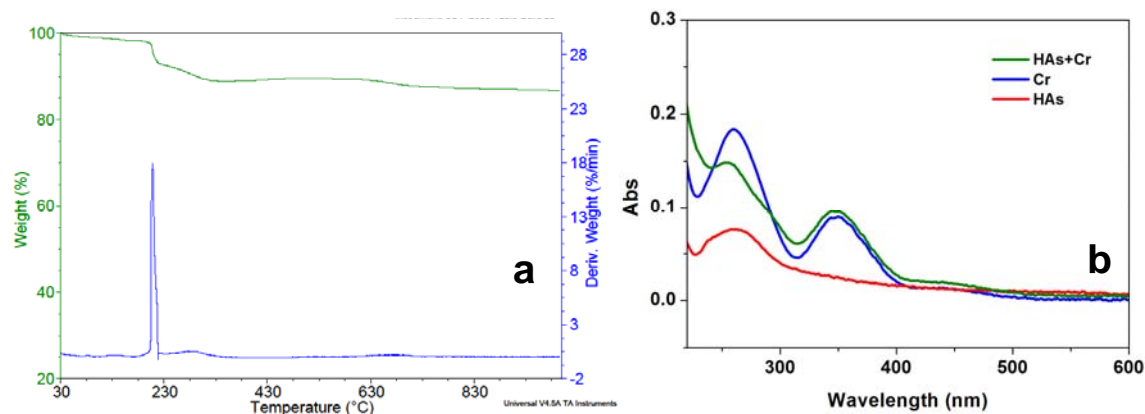

Figure 4 TG/DTG curves of $AuPtPd-Fe_3O_4$ nanocomposite (a). The UV–vis absorption spectra of Cr, HAs and the HAs+Cr mixture (b)

Two intense absorption bands at 260 and 348 nm can be seen in the UV–vis spectra of chromium, these bands were assigned to O-Cr(VI) electronic charge transfer of $Cr_2O_7^{2-}$ (Leita et al., 2009). The UV–vis absorbance spectra of HAs mainly come from the electronic charge transfer of aromatic ring structures and color-absorbing groups (Schaumann et al., 2011). It can be seen from the absorbance spectra of chromium-humic acids mixture that absorbance bands coming from aromatic ring structures in HAs decreased. The peak at 350 nm corresponds to the slight red shift of peak at 348 nm of Cr(VI), implied that HAs promoted the probability of intermolecular O-Cr(VI) electronic charge transfer together with an energetic benefit (Leita et al., 2009). In addition, no significant absorption band at 425 nm, assigned to the typical octahedral Cr(III) structure, can be seen. This implies that the reduction of Cr(VI) to Cr(III) was not occurred during the preparation of the test mixture. Calibration equations (Figure 5a,b) derived from calibration curves were plotted for the removal evaluation of Cr(VI) and HAs in water samples.
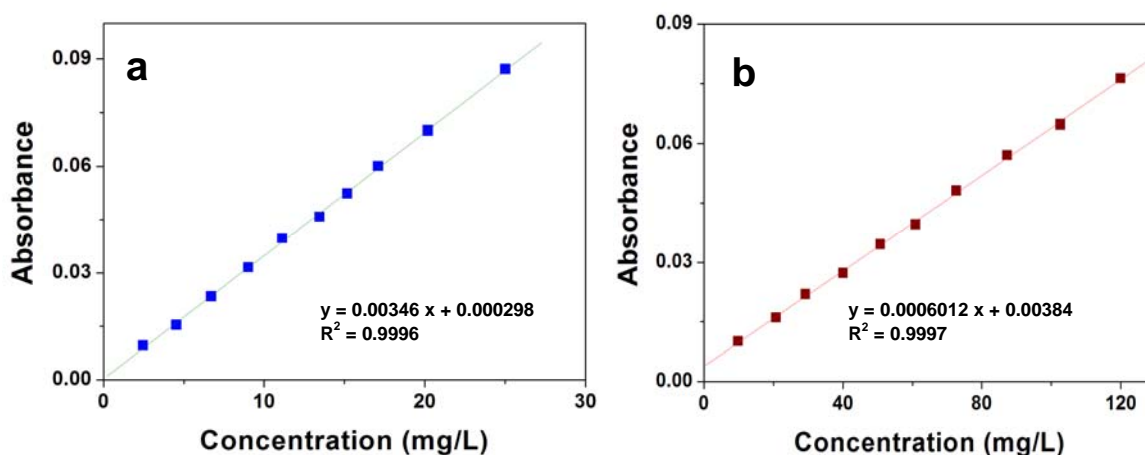

Figure 5 Absorbance/concentrations profiles of Cr (a) and HAs (b) at different concentrations

Good linearity is observed for both analytes throughout the concentration ranges of 2.5 to 25 mg/L and 12 to 120 mg/L for Cr and HAs respectively, with R^2 close to 1 in both cases (0.9996 for Cr and 0.9997 for HAs). For HAs and Cr electrolysis: pH 3.0, 30 mA, 0.8 g of $AuPtPd-Fe_3O_4$, 125 mg/L HAs and 25 mg/L Cr (VI), were used. The results are shown in Figure 6a and 6b. Excellent removal efficiency for total Cr was shown, see

Figure 6a. In particular, ~79% of total Cr was removed in 30 min, while ~99 % of total Cr was removed in 3 h. It was evident that ~95% of TOC was removed after 3 h electrolysis, indicating a quite complete mineralization to CO_2 of HAs, see Figure 6b.

The behaviour shown by AuPtPd-Fe_3O_4 evidences the beneficial effect of Au and Pt, probably due to an improved selectivity of the catalyst surface to form H_2O_2 instead of H_2 combustion (Sterchele et al., 2013; Sarno et al., 2018a). These results confirm the effectiveness of the electro-Fenton process in the simultaneous removal of HAs and Cr(VI). The high efficiency of our nanocatalyst can be ascribed to the effective catalytic activity of the Au/Pt/Pd nanoparticles during atomic hydrogen formation on the catalyst surface, in which Au and Pt presence probably favour the conversion of H_2 and O_2 to generate dissolved OH (Sterchele et al., 2013; Sarno et al., 2018a).
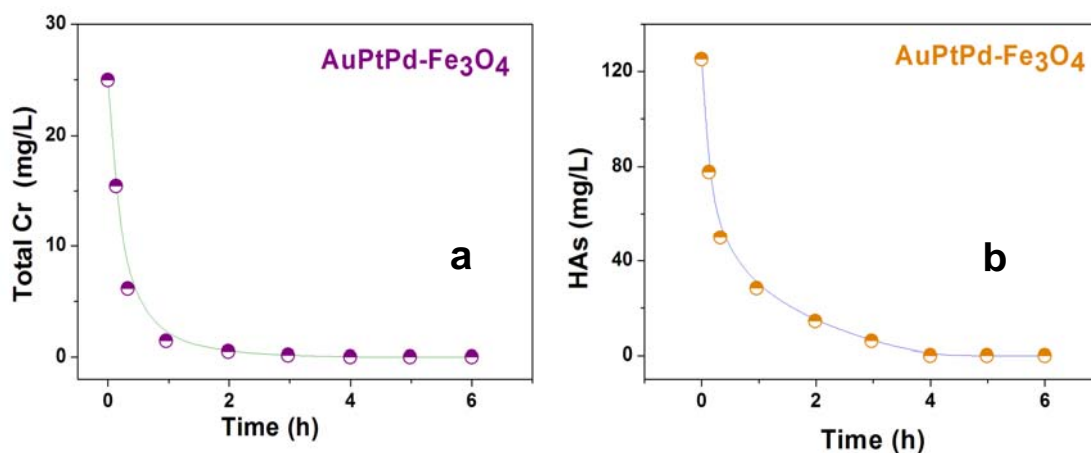

Figure 6 Total Cr evolution as a function of time during electro-Fenton process (a) and HAs evolution as a function of time during degradation (b).

4. Conclusions

A flower-like AuPtPd-Fe_3O_4 NPs nanocatalyst, consisting of faceted AuPtPd NPs on a quasi-spherical, 16.9 nm mean size, Fe_3O_4 NPs has been prepared, by an efficient and facile one pot synthesis process, for the effective and simultaneous removal of HAs and Cr (VI). To favour the dispersion of the nanoparticles in the electrochemical medium a ligand exchange was designed and tested. The alloy formation between Pt and Pd, based on the substitution of the Pt lattice sites, was confirmed by XRD analysis, on the other hand the peaks of the Au crystal faces are clearly visible. Calibration equations derived from calibration curves were plotted for the removal evaluation of Cr(VI) and HAs in water samples. Good linearity was observed for both analytes throughout the concentration ranges chosen. Effective and simultaneous removal of HAs and Cr(VI) has been achieved by the developed electro-Fenton process, where H_2O_2 was in situ electro-generated by combination of H_2 and O_2 on the Pd catalyst surface. Under the conditions of solution: pH 3.0, 30 mA, 125 mg/L HAs and 0.8 g of AuPtPd-Fe_3O_4, HAs were highly mineralized with TOC removal efficiency of 95% after only 3 h electrolysis, while ~99 % of total Cr was removed in 3 h. The homogeneous characteristics of the hydroxyl radicals produced by the electro-Fenton process determines their higher degradation efficiency on the respect of the anodic oxidation, suppling a more effective and safe way of H_2O_2 addition. The high efficiency of our nanocatalyst can be ascribed to the effective catalytic activity of the Au/Pt/Pd nanoparticles, due to Pt presence and highlighted by Au, which favour the conversion of H_2 and O_2 to generate dissolved OH even more homogeneously distributed in the medium.

References

Arai H., Arai M., Sakumoto A., 1986, Exhaustive degradation of humic acid in water by simultaneous application of radiation and ozone, Water Research, 20, 885–891.

Ban C., Wu Z., Gillaspie D.T., Chen L., Yan Y., Blackburn J.L., Dillon A.C., 2010, Nanostructured Fe_3O_4/SWNT electrode: binder-free and high-rate Li-Ion anode, Advanced Materials, 22, E145–E149.

Celebi M., Yurderi M., Bulut A., Kaya M., Zahmakiran M., 2016, Palladium nanoparticles supported on amine-functionalized SiO2 for the catalytic hexavalent chromium reduction, Applied Catalysis B: Environmental, 180, 53–64.

Chen J., LeBoeuf E.J., Dai S., Gu B., 2003, Fluorescence spectroscopic studies of natural organic matter fractions, Chemosphere, 50, 639–647.

Ciambelli P., Sannino D., Sarno M., Fonseca A., Nagy J.B., 2004, Hydrocarbon Decomposition in Alumina Membrane: An Effective Way to Produce Carbon Nanotubes Bundles, Journal of Nanoscience and Nanotechnology, 4, 779–787.

Costa A.S., Passos E.D.A., Garcia C.A.B., Alves J.D.P.H., 2011, Characterization of dissolved organic matter in the Piauí river estuary, Northeast Brazil, Journal of the Brazilian Chemical Society, 22, 2139–2147.

Ferrara M., Neitzert H.-C., Sarno M., Gorrasi G., Sannino D., Vittoria V., Ciambelli P., 2007, Influence of the electrical field applied during thermal cycling on the conductivity of LLDPE/CNT composites, Physica E: Low-dimensional Systems and Nanostructures, 37, 66–71.

Ghandoor H.E., Zidan H.M., Khalil M.M.H., Ismail M.I.M., 2012, Synthesis and some physical properties of magnetite (Fe_3O_4) nanoparticles, International journal of electrochemical science, 7, 5734–5745.

Gil R. A., Cerutti S., G'asquez J. A., Olsina R.A., Martinez L.D., 2006, Preconcentration andspeciation of chromium in drinking water samples by coupling of online sorption on activated carbon toetaas determination, Atlanta, 1065, 1065–1070.

Kinniburgh D.G., Milne C.J., Benedetti M.F., Pinheiro J.P., Filius J., Koopal L.K., van Riemsdijk W.H., 1996, Metal ion binding by humic acid: application of the NICA-Donnan model, Environmental Science & Technology, 30, 1687–1698.

Leita L., Margon A., Pastrello A., Arcon I., Contin M., Mosetti D., 2009, Soil humic acids may favour the persistence of hexavalent chromium in soil, Environmental Pollution, 157, 1862–1866.

Lin J., Zhan Y., 2012, Adsorption of humic acid from aqueous solution onto unmodified and surfactant-modified chitosan/zeolite composites, Chemical Engineering Journal, 200-202, 202–213.

Ren X., Song Y., Liu A., Zhang J., Yang P., Zhang J., An M., 2015, Experimental and theoretical studies of DMH as a complexing agent for a cyanide-free gold electroplating electrolyte, RSC Advances, 5, 64997–65004.

Sarno M., Iuliano M., 2018b, Highly active and stable Fe_3O_4/Au nanoparticles supporting lipase catalyst for biodiesel production from waste tomato, Applied Surface Science, in press. DOI: 10.1016/j.apsusc.2018.04.060.

Sarno M., Iuliano M., Polichetti M., Ciambelli P., 2017a, High activity and selectivity immobilized lipase on Fe_3O_4 nanoparticles for banana flavour synthesis, Process Biochemistry, 56, 98–108.

Sarno M., Ponticorvo E., 2017b, Much enhanced electrocatalysis of Pt/PtO_2 and low platinum loading Pt/PtO_2-Fe_3O_4 dumbbell nanoparticles, International Journal of Hydrogen Energy, 42, 23631–23638.

Sarno M., Ponticorvo E., 2018a, Pt/Pd-Fe_3O_4 nanoparticles for removal of humic acids and Cr(VI), Chemical Engineering Transactions, 68, 469–474.

Sarno M., Ponticorvo E., 2018c, Continuous flow HER and MOR evaluation of a new Pt/Pd/Co nano electrocatalyst, Applied Surface Science, 459,105–113.

Schaumann G.E., Thiele-Bruhn S., 2011, Molecular modeling of soil organic matter: Squaring the circle?, Geoderma,166, 1–14.

Sterchele S., Biasi P., Centomo P., Canton P., Campestrini S., Salmi T., Zecca M., 2013, Pd-Au and Pd-Pt catalysts for the direct synthesis of hydrogen peroxide in absence of selectivity enhancers, Applied Catalysis A: General, 468, 160-174.

Sun X., Zheng C., Zhang F., Yang Y., Wu G., Yu A., Guan N., 2009, Size-controlled synthesis of magnetite (Fe_3O_4) nanoparticles coated with glucose and gluconic acid from a single Fe(III) precursor by a sucrose bifunctional hydrothermal method, The Journal of Physical Chemistry C, 113, 16002–16008.

Trellu C., Péchaud Y., Oturan N., Mousset E., Huguenot D., van Hullebusch E.D., Esposito G., Oturan M.A., 2016, Comparative study on the removal of humic acids from drinking water by anodic oxidation and electro-Fenton processes: Mineralization efficiency and modelling, Applied Catalysis B: Environmental, 194, 32–41.

Trezza M., Prischepa S.L., Cirillo C., Fittipaldi R., Sarno M., Sannino D., Ciambelli P., Hesselberth M.B.S., Lazarouk S.K., Dolbik A.V., Borisenko V.E., Attanasio C., 2008, Superconducting properties of Nb thin films deposited on porous silicon templates, Journal of Applied Physics, 104, 083917.

Wang L., Han C., Nadagouda M.N., Dionysiou D.D., 2016, An innovative zinc oxide-coated zeolite adsorbent for removal of humic acid, Journal of Hazardous Materials, 313, 283–290.

Wang L., Yamauchi Y., 2011, Strategic Synthesis of Trimetallic Au@Pd@Pt Core−Shell Nanoparticles from Poly(vinylpyrrolidone)-Based Aqueous Solution toward Highly Active Electrocatalysts, Chemistry of Materials, 23, 2457–2465.

Xu Z., Shen C., Hou Y., Gao H., Sun S., 2009, Oleylamine as both reducing agent and stabilizer in a facile synthesis of magnetite nanoparticles, Chemistry of Materials, 21, 1778–1780.